TITLE PAGE

Mode discrimination by lossy dielectric rods in cavities of second-harmonic gyrotrons

Vitalii I. Shcherbinin[1,2*] (0000-0002-9879-208X)
Konstantinos A. Avramidis[1] (0000-0001-9493-0468),
Manfred Thumm[1,3] (0000-0003-1909-3166)
John Jelonnek[1,3] (0000-0002-0531-7600)

[1]Institute for Pulsed Power and Microwave Technology, Karlsruhe Institute of Technology, 76131 Karlsruhe, Germany
[2]National Science Center "Kharkiv Institute of Physics and Technology", 61108 Kharkiv, Ukraine
[3]Institute of Radio Frequency Engineering and Electronics, Karlsruhe Institute of Technology, 76131 Karlsruhe, Germany
*e-mail: vshch@ukr.net

Abstract The influence of a coaxial dielectric rod on eigenvalues, ohmic losses, transverse field structure and beam-wave coupling coefficients is investigated for TE modes of a gyrotron cavity. It is shown that such dielectric insert, when made from a moderate-loss material, results in strong attenuation of all cavity modes, with the exception of those having caustic radii much larger than the insert radius. It is proposed to employ such dielectric loading for selective suppression of competing modes in cavities of second-harmonic gyrotrons. The high performance and flexibility of the proposed method of mode discrimination is demonstrated for the example of the cavity of the high-power 0.39-GHz second-harmonic gyrotron developed at the University of Fukui. In addition, some fascinating capabilities enabled by coaxial inserts made of ultralow-loss dielectrics are discussed.

Keywords gyrotron, cyclotron harmonic, cavity, mode selection, dielectric loading

Declarations

Funding Partial financial support was received from the Alexander von Humboldt Foundation.

Conflicts of interest/Competing interests The authors have no conflicts of interest to declare that are relevant to the content of this article.

Availability of data and material Data are available from the authors upon reasonable request.

Mode discrimination by lossy dielectric rods in cavities of second-harmonic gyrotrons

Vitalii I. Shcherbinin[1,2*], Konstantinos A. Avramidis[1], Manfred Thumm[1,3], and John Jelonnek[1,3]

[1]Institute for Pulsed Power and Microwave Technology, Karlsruhe Institute of Technology, 76131 Karlsruhe, Germany
[2]National Science Center "Kharkiv Institute of Physics and Technology", 61108 Kharkiv, Ukraine
[3]Institute of Radio Frequency Engineering and Electronics, Karlsruhe Institute of Technology, 76131 Karlsruhe, Germany
*e-mail: vshch@ukr.net

Abstract The influence of a coaxial dielectric rod on eigenvalues, ohmic losses, transverse field structure and beam-wave coupling coefficients is investigated for TE modes of a gyrotron cavity. It is shown that such dielectric insert, when made from a moderate-loss material, results in strong attenuation of all cavity modes, with the exception of those having caustic radii much larger than the insert radius. It is proposed to employ such dielectric loading for selective suppression of competing modes in cavities of second-harmonic gyrotrons. The high performance and flexibility of the proposed method of mode discrimination is demonstrated for the example of the cavity of the high-power 0.39-GHz second-harmonic gyrotron developed at the University of Fukui. In addition, some fascinating capabilities enabled by coaxial inserts made of ultralow-loss dielectrics are discussed.

Keywords gyrotron, cyclotron harmonic, cavity, mode selection, dielectric loading

1. Introduction

It is common knowledge that harmonic mode competition is a limiting factor, which hinders progress in the development of high-performance second-harmonic gyrotrons for a wide variety of modern applications, especially in the sub-terahertz-to-terahertz frequency band [1-5]. That is the reason why suppression of the first-harmonic modes in gyrotron cavities presents a vital and topical issue. To solve this issue, a number of improved gyrotron cavities have been considered so far. Among them, to name just a few, are iris-loaded cavities [6-8], complex-cavities [9, 10], cavities with phase correctors [11] or output reflector [12], dielectric-coated [13] and corrugated [14, 15] cavities. A special type of improved gyrotron cavities involves coaxial cavities for second-harmonic gyrotrons [16-19]. In these cavities, mode suppression by losses is applied, relying on dissimilar sensitivity of different cavity modes to a coaxial insert.

Coaxial gyrotron cavities can be roughly divided into two classes, depending on the kind of losses applied to discriminate against competing modes. The first (and widest) class of cavities, which also find use in first-harmonic gyrotrons [20, 21], employs nonuniform inserts to increase the diffraction losses of the competing modes [16, 18, 19]. The best-known example of such an insert is a down-tapered conducting rod with longitudinal subwavelength impedance corrugations [16, 22-24]. Additional improvement of selectivity properties of gyrotron cavities can be achieved for coaxial inserts with step nonuniformities, which make it possible to reduce the effective cavity length of competing modes [18, 19]. Such an improvement is particularly important for broadband second-harmonic gyrotrons [25-28], in which the risk of competition from high-order axial modes is high [3, 18]. The highly versatile method of mode discrimination in cavities of second-harmonic gyrotrons is that provided by a coaxial metal rod partially coated by a low-loss dielectric layer. As shown in [19], this method enables efficient suppression of all first- and second-harmonic competing modes having smaller caustic radii than that of the operating mode.

Such beneficial property is also inherent in second class of coaxial cavities, which employ resistive (purely conducting) inserts to increase ohmic losses of the competing modes [16, 17, 23, 29]. Despite this benefit, such inserts, on the one hand, need to possess very low conductivity to ensure efficient suppression of high-order axial competing modes with high diffraction losses. On the other hand, the insert material must exhibit a high enough conductivity to behave like a conductor [30]. In practice, such a contradiction can severely constrain the choice of an appropriate resistive material for use in coaxial cavities of sub-terahertz second-harmonic gyrotrons. For such use, an alternative design solution in the form of a coaxial all-dielectric rod with moderate losses is considered in this paper. To be efficient, such a design solution requires the operating gyrotron mode to have relatively large caustic radius. A concrete example can be provided by the operating $TE_{17,2}$ mode of the 0.39-THz second-harmonic gyrotron developed at the University of Fukui (FIR-UF) [4, 31]. Experiments show that the operating performance of this gyrotron is impaired by competition between the operating and first-harmonic modes.

The paper is organized as follows. In Section II, the dispersion relation for quasi-TE modes near cutoff frequencies of a cylindrical metal waveguide loaded with a coaxial dielectric rod is derived. For these modes the influence of the dielectric loading on frequencies, ohmic losses, and field distribution is investigated. In Section III, the use of a coaxial dielectric insert with moderate losses is considered for efficient discrimination against competing modes in gyrotron cavities. Such a benefit of a dielectric loading is illustrated by the example of the cavity for the 0.39-THz second-harmonic gyrotron of FIR-UF. In Section IV, the possibility of loss compensation in gyrotron cavities by ultralow-loss dielectric inserts is discussed. In the last section, the results of the investigation are summarized.

2. Vacuum and dielectric modes

In gyrotron cavities, the basis modes are orthogonal normal modes of a uniform waveguide. Therefore, first we consider a hollow cylindrical waveguide with constant radius R. The waveguide is made of a conducting material and incorporates a coaxial dielectric rod with radius R_i and complex relative permittivity ε (Fig. 1). Assume that the waveguide

eigenfrequencies are close to cutoff frequencies. In this case, a dielectric-loaded waveguide is characterized by weakly-coupled TE and TM eigenmodes [32-34].

Let us consider (quasi-) TE modes ($|E_z/H_z| << 1$). In cylindrical coordinates $\{r, \varphi, z\}$, their fields can be written as

$$
\begin{aligned}
&H_z = f(z) h_z(r) = f(z) \begin{cases} k_\perp^2 \psi(r), & R_i < r < R \\ k_d^2 \psi(r), & r < R_i \end{cases} \\
&\mathbf{E}_\perp = f(z) \mathbf{e}_\perp(r), \ \mathbf{H}_\perp = k^{-1} f'(z) \mathbf{h}_\perp(r) \\
&e_\varphi(r) = -i h_r(r) = -ik \frac{d\psi}{dr}, \\
&e_r(r) = i h_\varphi(r) = -k \frac{m}{r} \psi \\
&\psi(r) = \begin{cases} A Z_m(k_\perp r), & R_i < r < R \\ B J_m(k_d r), & r < R_i \end{cases}
\end{aligned}
\tag{1}
$$

where $f(z) = \exp(ik_z z)$, k_z is the axial wavenumber, $k = \omega/c$, ω is the mode angular frequency, c is the speed of light in vacuum, $k_\perp^2 = k^2 - k_z^2$, $k_d^2 = \varepsilon k^2 - k_z^2$, $\varepsilon = \varepsilon_r(1 + i \tan\delta)$, $\varepsilon_r = \mathrm{Re}\,\varepsilon$, $\tan\delta = \sigma_i / (\varepsilon_r \varepsilon_0 \omega)$ is the loss tangent of the dielectric rod, σ_i is the real-valued effective conductivity of the coaxial insert, m is the azimuthal mode index, $Z_m(k_\perp r) = [J_m(k_\perp r) + A_0 N_m(k_\perp r)]$, $J_m(\cdot)$ and $N_m(\cdot)$ are the m-th order Bessel and Neumann functions, respectively, constants A, B and A_0 are as yet unknown, the field factor $\exp(-i\omega t + im\varphi)$ is assumed and omitted.

To find the unknown constants we substitute $e_\varphi(r)$ and $h_z(r)$ into the boundary conditions

$$
\left.\frac{e_\varphi}{h_z}\right|_{r=R} = Z_s, \ \left.\frac{e_\varphi}{h_z}\right|_{r=R_i} = -\eta_\varphi = -\frac{ik}{k_d} \frac{J_m'(k_d R_i)}{J_m(k_d R_i)}
\tag{2}
$$

where $Z_s = -ikd_c$ is the impedance of a conducting surface $r = R$, $d_c = (1+i)d/2$, $d = \sqrt{2/(\mu_0 \omega \sigma)}$ is the skin-depth, and σ is the wall conductivity [35].

This leads to the following dispersion relation:

$$
\frac{kJ_m'(k_\perp R) - ik_\perp Z_s J_m(k_\perp R)}{kJ_m'(k_\perp R_i) + ik_\perp \eta_\varphi J_m(k_\perp R_i)} = \frac{kN_m'(k_\perp R) - ik_\perp Z_s N_m(k_\perp R)}{kN_m'(k_\perp R_i) + ik_\perp \eta_\varphi N_m(k_\perp R_i)}
\tag{3}
$$

which yields the complex eigenvalues $k_\perp R = \chi_{mn}(1 - i/(2Q_{ohm}))$ of $\mathrm{TE}_{m,n}$ modes of dielectric-loaded waveguides near cutoff frequencies ($|k_z^2/k^2| << 1$) and is identical to that presented in [36]. Note that, in deriving (3), we reduce the continuity conditions for $e_\varphi(r)$ and $h_z(r)$ at the vacuum-dielectric interface $r = R_i$ to the one-side (impedance-like) boundary condition (2) [37]. In the limiting case of a coaxial rod made of high-conductivity material ($\tan\delta >> 1$), one obtains $\varepsilon \approx i\sigma_i/(\varepsilon_0 \omega)$ and $\eta_\varphi \approx 1/\sqrt{\varepsilon}$ [30]. In this case, dispersion relation (3) takes the well-known form for an all-metal coaxial waveguide [29], while condition $\tan\delta = \sigma_i/(\varepsilon_r \varepsilon_0 \omega) >> 1$ imposes a lower limit on the conductivity σ_i for the resistive coaxial inserts considered in [16, 17, 23, 29]. It is obvious that this limit is linear with frequency.

Our prime interest is in the effect of a lossy dielectric insert on the waveguide modes. Despite this, for completeness we first neglect dielectric losses ($\tan\delta = 0$). Fig. 2 demonstrates typical solutions of the characteristic equation (3) for a cylindrical metal waveguide loaded with a lossless coaxial dielectric rod. In this figure, the characters m,n and m,nd are used to denote $\mathrm{TE}_{m,n}$ modes of the dielectric-loaded waveguide in the extreme cases of $R_i = 0$ ($C = \infty$) and $R_i = R$ ($C = 1$), respectively. In the calculations, the following parameters are used: $R = 2.99$ mm, $m = 6$, $\varepsilon_r = 9$, $\tan\delta = 0$, $\sigma = 2.9 \times 10^7$ S/m (half the DC conductivity of OFHC copper). As may be seen from Fig. 2a, for $R_i = 0$ the solutions of the dispersion relation are eigenvalues of TE modes of a hollow cylindrical waveguide with finite wall conductivity, i.e. χ_{mn} are close to zeros μ_{mn} of the function $J_m'(\cdot)$ for $|Z_s| << 1$. In this case, ohmic losses in the conducting wall are solely responsible for attenuation of guided modes. In the opposite extreme case $R_i = R$, equation (3) yields eigenvalues of a conducting cylindrical waveguide completely filled with dielectric, i.e. $\chi_{mn} \approx \mu_{mn}/\sqrt{\varepsilon_r}$. In this case, dielectric losses are expected to make an additional contribution to mode attenuation. In the following, the eigenmodes of a dielectric-loaded

waveguide will be called vacuum or dielectric modes, depending on whether their fields are mainly localized inside the vacuum ($R_i < r < R$) or dielectric ($r \le R_i$) regions. Obviously, for $R_i = 0$ and $R_i = R$ we deal with pure vacuum and dielectric modes, respectively.

As the radius ratio $C = R/R_i$ starts to grow from unity and the volume of the dielectric rod decreases, the eigenvalues of dielectric modes increase and thereby approach those of vacuum modes. At the same time, the eigenvalues of vacuum $TE_{m,n}$ modes are slightly affected by the dielectric rod, provided that the rod radius R_i is distinctly smaller than the mode caustic radii $R_{m,n} = R|m|/\mu_{mn}$. Exceptions are certain frequency ranges, where the eigenvalues of dielectric and vacuum modes approach each other. In these ranges, interaction between dielectric and vacuum modes takes place. Such mode interaction gives rise to TE modes in the form of a mixture of vacuum and dielectric modes.

To illustrate this more clearly, we depict the field distribution (Fig. 3) for guided modes having eigenvalues, which are shown by symbols 1-4 in Fig. 2. Fig. 3a corresponds to the eigenvalue 1, which is close to μ_{62} . In this case, the TE mode of the dielectric-loaded waveguide is the vacuum mode having an electromagnetic field, which is mainly concentrated inside the vacuum channel. Therefore, the ohmic Q-value of this mode is close to that of the $TE_{6,2}$ mode of a hollow metal waveguide (Fig. 2b). Figs. 3c and 3d correspond to equal eigenvalues 3 and 4, which are attained for different radii R_i . It can be seen that these eigenvalues belong to dielectric modes, which exhibit field concentration inside the dielectric rod. As a consequence, the electromagnetic fields of such modes have rather small amplitudes near the metal surface $r = R$. For this reason, in the dielectric-loaded metal waveguide, dielectric modes are only slightly sensitive to wall conductivity and can have very low attenuation (Fig. 2b), provided that the loss tangent $\tan\delta$ is small enough. In this sense, these modes are similar to the so-called "inner mode", which is the eigenmode of an all-metal coaxial waveguide with a corrugated inner conductor which exhibits low ohmic losses in the outer waveguide wall [38]. The eigenvalue 2 arises from interaction of vacuum and dielectric modes. For this eigenvalue an electromagnetic field of the guided TE mode possesses properties of both vacuum and dielectric modes and thus has a distinct amplitude inside the entire volume of the waveguide (Fig. 3b). That is the reason why this mode intermediates in ohmic Q-value between the vacuum and dielectric modes (Fig. 2b).

We next focus our attention on the ability of a coaxial rod made of a lossy dielectric to suppress guided TE modes. In a dielectric-loaded gyrotron cavity, these modes can compete with each other. The effect of loss tangent $\tan\delta$ on the ohmic Q-value of the dielectric-loaded metal waveguide is shown in Fig. 4a. It is not surprising that this effect is most pronounced for dielectric modes, which can be strongly damped even with a low-loss ($\tan\delta < 0.01$) dielectric loading. Therefore, even though these modes are additional competing modes introduced by the insert, they are less dangerous competitors than vacuum modes. To discriminate against the vacuum $TE_{m,n}$ modes of a dielectric-loaded gyrotron cavity one needs to make the radius R_i of the lossy dielectric rod close to or larger than their caustic radii $R_{m,n}$. In the next section, this property of a coaxial dielectric insert will be applied to discriminate against competing modes in the cavity of the 0.39-THz second-harmonic gyrotron developed at FIR-UF for use in the collective Thomson scattering (CTS) diagnostics of fusion plasmas [4, 31].

3. Mode discrimination

The FIR-UF 0.39-THz second-harmonic gyrotron has been operated in the whispering-gallery $TE_{17,2}$ mode which has a relatively large caustic radius $R_{17,2} \approx 0.7R$. The gyrotron is originally equipped with a conventional hollow cylindrical cavity and has the following electron beam parameters: beam voltage $V_b = 60$ kV, beam current $I_b = 10$ A, pitch factor $\alpha = 1.2$, and beam radius $r_b = 0.195$ cm [4, 31]. The gyrotron cavity is made of copper and consists of input, central (main) and output sections having the lengths $L_1 = 5$ mm, $L_2 = 12$ mm, and $L_3 = 5$ mm and taper angles $\theta_1 = 1.5°$, $\theta_2 = 0$, and $\theta_3 = 3°$, respectively. The radius R of the cylindrical main section equals 2.99 mm. The assumed electrical conductivity $\sigma = 2.9\times10^7$ S/m of the cavity wall is one-half the DC value of ideal OFHC copper. The ohmic and diffractive quality factors of the operating mode in the cold cavity equal 10270 and $9870/q^2$, respectively, where q is the axial mode index. In simulations, we neglect the velocity spread of beam electrons [31] and rely on the self-consistent single-mode code KIPT [35].

Fig. 5 shows the starting currents of the operating and competing TE modes of the 0.39-THz second-harmonic gyrotron. It can be seen that the gyrotron features a relatively dense spectrum of competing modes. Among these competitors, first-harmonic modes look particularly dangerous. Besides it is important to keep in mind that the information provided by Fig. 5 is incomplete and gives no evidence of the hard-excitation regions for competing modes. In such a region, oscillation of a competing mode is possible, even though its starting current exceeds the operating beam current. According to experimental observations [4], in the 0.39-THz second-harmonic gyrotron, this is the case for the first-harmonic $TE_{4,3}$ mode, which is first excited in the hard-excitation region due to nonlinear interaction with the operating second-harmonic $TE_{17,2}$ mode and then suppresses the operating mode. As reported in [31], this effect presents a "*latent limiting factor for attaining higher power*" of the 0.39-THz second-harmonic gyrotron and thus hinders its use in CTS diagnostics. Obviously, this limitation can only be overcome by suppressing all dangerous competing modes. As Fig. 5 suggests, for the 0.39-THz second-harmonic gyrotron such modes are volume modes with relatively small caustic radii.

To improve mode selection we propose to equip the cavity of the 0.39-THz second-harmonic gyrotron with a uniform dielectric rod characterized by moderate losses ($\tan\delta < 0.1$). Such a rod can be fabricated from commercial AlN-SiC (or

BeO-SiC) ceramics, which can possess loss tangent in the wide range from 0.001 to 0.5 depending on volume fraction of SiC [34, 39, 40]. Benefits of these ceramics are vacuum compatibility and exceptionally high thermal conductivity, which make such dielectrics suitable for use in high-power vacuum devices [41, 42]. The radius of the lossy dielectric rod must be selected sufficiently small to have only a slight effect on the operating mode. The required value of R_i is determined by the mode caustic radius and depends on ε_r (Fig. 6). For definiteness, we set $\varepsilon_r = 9$ and $\tan\delta = 0.05$. In this case, Fig. 6 suggests that the $TE_{17,2}$ mode of the gyrotron cavity is slightly sensitive to a coaxial dielectric rod, provided that the condition $C > 2.3$ is fulfilled. Under this condition, the fabrication imperfections and misalignment of the rod have little or no effect on the operating mode. It should be emphasized that even though the chosen parameters $\varepsilon_r = 9$ and $\tan\delta = 0.05$ of the dielectric material can only be considered as typical characteristics, our design consideration can be easily adjusted to an actual ceramic rod, once its complex permittivity is measured in the frequency range of interest.

In general, for suppression of competing modes by a lossy coaxial rod in a gyrotron cavity it is reasonable to select R_i as large as possible [16, 17, 23, 29]. For this reason, we first consider a uniform dielectric rod with $\varepsilon_r = 9$, $\tan\delta = 0.05$ and constant radius $R_i = 1.3$ mm ($C = 2.3$ for $R = 2.99$ mm). Table I demonstrates the influence of such a rod on the complex eigenvalues of a cylindrical metal waveguide with radius $R = 2.99$ mm. Note that we henceforth use the same labeling of the waveguide modes for any R_i and are concerned only with those competing modes, which are capable of oscillating in the operating range of the 0.39-THz second-harmonic gyrotron. As may be seen from Table I, a lossy dielectric rod can well discriminate against competing modes with small caustic radii. To be more specific, the ohmic Q-value of the most dangerous competing $TE_{4,3}$ mode is reduced more than 300 times due to the presence of the designed coaxial insert in the cavity of the 0.39-THz second-harmonic gyrotron. An important point is that this effect is achieved for a dielectric rod with relatively small loss tangent. This opens up a wide variety of suitable dielectrics and offers opportunities for selection of the most appropriate material with desirable vacuum, mechanical, thermal and charging properties. Such a benefit distinguishes the proposed method of mode discrimination in gyrotron cavities from that provided by resistive rods [16, 17, 23, 29] for which the search for suitable metal-like materials can be a challenging task. Similar restriction is also inherent in a good-conducting coaxial cavity with an insert partially coated by a thin dielectric layer [19], which can only be made from a limited number of dielectric materials. Moreover, contrary to [16, 17, 19, 23, 29], we propose to equip the gyrotron cavity with a uniform coaxial insert, which can be more easily fabricated to close tolerances and causes no or little mode conversion. Note that although the effect of mode conversion is well-known [43-47], its influence on the beam-wave interaction in gyrotron cavities still remains poorly explored [48].

To investigate the beam-wave interaction in a dielectric-loaded gyrotron cavity we have modified the code KIPT in order to take into account the effect of a coaxial dielectric insert on cavity eigenvalues (see (3)) and coefficients of the beam coupling with the TE_{mn} modes

$$C_{mn} = \frac{Z_{m-s}^2\left(k_\perp r_b\right)}{2\int_0^R rdr\left[\psi'^2 + m^2 r^{-2}\psi^2\right]} \tag{4}$$

where r_b is the beam radius, s is the number of cyclotron harmonic, $\psi' = d\psi/dr$. In the extreme case $R_i = 0$ and $Z_s = 0$, the coefficient (4) takes the well-known form $C_{mn} = J_{m-s}^2\left(k_\perp r_b\right)\Big/\left[\left(\mu_{mn}^2 - m^2\right)J_m^2\left(\mu_{mn}\right)\right]$ for a hollow cylindrical gyrotron cavity made of perfect electric conductor [49].

Fig. 7a shows the starting currents of the operating $TE_{17,2}$ mode and competing modes of the 0.39-THz second-harmonic gyrotron equipped with the dielectric-loaded cavity for $\varepsilon_r = 9$, $\tan\delta = 0.05$ and $R_i = 1.3$ mm. With reference to Figs. 5 and 7a, it can be seen that the lossy dielectric rod discriminates against all competing modes with the exception of those having large caustic radii. Moreover, among the remaining unsuppressed modes only the first-harmonic $TE_{6,2}$ mode can be recognized as dangerous competitor. As may be seen from Table I, the lossy dielectric loading of the gyrotron cavity provides nearly a 100-fold decrease in the ohmic Q-value of this mode. Despite such a strong effect, the increased ohmic losses in the cavity of the 0.39-THz second-harmonic gyrotron are inadequate to completely suppress the high-order axial $TE_{6,2}$ mode because of its low diffraction Q-value [28]. In theory, the most direct and clear way to discriminate against this competitor is to increase the loss tangent of the dielectric insert. This can be seen from Fig. 8. From Figs. 7a and 8 it becomes evident that the operating $TE_{17,2}$ mode of the 0.39-THz second-harmonic gyrotron dominates over the remaining competing modes in a wide frequency range, provided that the loss tangent $\tan\delta$ is increased up to 0.07 for the dielectric insert with $\varepsilon_r = 9$ and $R_i = 1.3$ mm. In this case, the dielectric-loaded cavity for the 0.39-THz second-harmonic gyrotron meets the design goal, even though the increased dielectric losses still remain much lower than those usually employed to suppress parasitic modes in interaction structures and beam tunnels of gyro-devices [41, 42, 50, 51].

Noteworthy also is another design solution. From the eigenfrequency analysis (see also Figs. 2 and 4a) follows that the ohmic losses of the first-harmonic $TE_{6,2}$ mode can be increased by reducing the insert radius R_i below 1.3 cm. In this process, however, the ohmic Q-values of the less dangerous second-harmonic $TE_{13,3}$ and $TE_{14,3}$ modes increase, while the frequency of the strongly attenuated dielectric mode, which is henceforth designated as $TE_{6,2d}$ mode, approaches that of the

$TE_{6,2}$ mode (Fig. 2). A compromise can be reached for $R_i = 1.18$ mm ($C = 2.54$ for $R = 2.99$ mm). For this insert, the ohmic Q-values of the $TE_{6,2}$, $TE_{6,2d}$, $TE_{13,3}$ and $TE_{14,3}$ modes can be found in Table I. As is seen from Fig. 7b, the resultant increase in the ohmic losses of the first-harmonic $TE_{6,2}$ mode makes this mode non-oscillating in the operating region of the 0.39-THz second-harmonic gyrotron. In this region, oscillation is possible for few second-harmonic competing modes. This problem, however, is believed to be not critical and can be avoided by a proper gyrotron start-up, e.g. for the fixed magnetic field $B_0 = 7.8$ T. Hence it follows that the alternative structure of a dielectric insert is also capable of removing a limitation on power increase in the 0.39-THz second-harmonic gyrotron for CTS diagnostics. This demonstrates that a coaxial dielectric rod with moderate losses provides a flexible means for efficient discrimination against competing modes in cavities of second-harmonic gyrotrons and can be easily optimized depending on design specifications on size and material of the coaxial insert. Besides it should be emphasized that a coaxial insert in coaxial-cavity gyrotrons usually extends from the gun region through the beam tunnel and the cavity [20, 21]. In such configuration, a lossy dielectric rod inserted into the beam tunnel may additionally offer a means of suppressing volume parasitic modes (e.g. $TE_{0,n}$ modes), which can sometimes deteriorate the gyrotron operation [50]. Such a bi-functional role of the coaxial dielectric loading may further improve the performance of sub-terahertz gyrotrons operated in second-harmonic modes.

4. High-Q dielectric modes

Of special note are also some fundamentally different capabilities, which can be offered by coaxial inserts made of dielectrics with ultralow losses. In the sub-terahertz frequency band, an example of such a dielectric is Chemical Vapor Deposition (CVD) diamond with $\varepsilon_r = 5.7$ [52] and loss tangents lying in the range from 3×10^{-6} to 2×10^{-5} [53, 54]. As is seen from Figs. 2 and 4a, dielectric modes of a metal waveguide with a ultralow-loss dielectric rod may have ohmic Q-values, which are several orders of magnitude higher than those for TE modes of a hollow metal waveguide ($R_i = 0$). This fascinating property can make high-Q dielectric modes particularly attractive as operating modes for broadband sub-THz gyrotrons, which suffer from extremely high ohmic losses in the cavity walls [25-27, 35]. For such a use in gyrotrons, however, the beam coupling with dielectric modes must be strong enough. At the same time, it might be supposed that this coupling is generally weak, since the fields of dielectric modes are mainly concentrated inside the dielectric insert (Figs. 3c and 3d), while a helical electron beam can only propagate inside the vacuum channel of the gyrotron cavity. To examine this supposition, we investigate the coefficient C_{mn} of the beam coupling with the $TE_{m,n}$ modes of a metal cylindrical waveguide loaded with a coaxial dielectric rod (see (4)).

Fig. 4b shows a variation of $\mathrm{Re}\,C_{mn}$ along the eigenfrequency curve, which is depicted by the dashed blue line in Fig. 2, for several values of the beam radius $r_b = R_i + C_b\left(R - R_i\right)$, where $0 < C_b < 1$. In this figure, $\mathrm{Re}\,C_{mn}$ is normalized by the maximal coefficient of the beam coupling with the $TE_{6,2}$ mode of a hollow cylindrical waveguide. It can be seen that, in the case of beam interaction with dielectric modes, the beam-wave coupling coefficient $\mathrm{Re}\,C_{mn}$ can even exceed this maximum, provided that C_b is small enough and thus the beam radius r_b is positioned relatively close to the radius R_i of the dielectric rod. In [36], a similar effect induced by a coaxial dielectric insert was shown to be responsible for strengthening the beam-wave coupling in cavities of high-harmonic large-orbit gyrotrons. Thus it may be inferred that, contrary to the expectations, strong coupling between a helical electron beam and dielectric modes is theoretically possible. This outcome gives promise that elimination of high ohmic losses in cavities of sub-terahertz and terahertz gyrotrons by ultralow-loss dielectric inserts can be feasible. To demonstrate the feasibility of such gyrotrons more conclusively, further extensive investigations are required. These investigations are currently under way.

5. Conclusion

The dispersion relation has been derived for TE modes guided near cutoff frequencies by a metal cylindrical waveguide loaded with a coaxial dielectric rod. Using this equation, the influence of the dielectric loading on complex mode eigenvalues has been investigated. Two types of guided TE modes have been shown to exist in the dielectric-loaded waveguide. One type involves vacuum modes, which originate from TE modes of a hollow cylindrical waveguide and can exist, provided that their caustic radii are distinctly larger than the radius of the coaxial dielectric insert. It has been shown that the fields of vacuum modes are mainly localized outside the dielectric insert, which slightly affects their ohmic losses. Modes of another type are dielectric modes. Their fields are concentrated inside the dielectric loading and decay towards the waveguide wall. Because of this property, ohmic losses of dielectric modes are little sensitive to losses in the waveguide wall and thus can be made extremely small or large, depending on the loss tangent of the dielectric loading. The ability of a lossy dielectric insert to suppress guided TE modes has been applied to discriminate against most dangerous competing modes in the cavity of the 0.39-THz second-harmonic gyrotron of FIR-UF. Simulations have shown that these competing modes can be strongly damped by coaxial dielectric rods of different constant radii, even though the dielectric losses employed are relatively low. This provides great flexibility in designing the coaxial inserts made from commercially available dielectrics for improved cavities of sub-terahertz second-harmonic gyrotrons. Such a design must take into consideration vacuum, mechanical and thermal properties of dielectric materials.

In addition, it has been demonstrated that coaxial inserts made of ultralow-loss dielectrics can support dielectric modes of the gyrotron cavity with ohmic Q-values, which are several orders of magnitude higher than those for modes a hollow metal cavity. The coupling of these modes with a helical electron beam has been shown to be sufficiently strong, provided

that the beam radius is placed close enough to the insert radius. This property, together with low attenuation, makes high-Q dielectric modes particularly attractive as operating modes for low-power broadband sub-terahertz and terahertz gyrotrons.

Acknowledgements The work of Vitalii I. Shcherbinin was supported by the Georg Forster Research Fellowship for Experienced Researchers from the Alexander von Humboldt Foundation.

References

1) T. Idehara, T. Tatsukawa, I. Ogawa, T. Mori, H. Tanabe, S. Wada, G. F. Brand, M. H. Brennan, Appl. Phys. Lett. (1991) http://dx.doi.org/10.1063/1.105135
2) V.L. Bratman, A.E. Fedotov, T. Idehara, Int. J. Infrared Millim. Waves (2001) http://dx.doi.org/10.1023/A:1015030405179
3) S.H. Kao, C.C. Chiu, K.F. Pao, K.R. Chu, Phys. Rev. Lett. (2011) http://dx.doi.org/10.1103/PhysRevLett.107.135101
4) T. Saito, Y. Tatematsu, Y. Yamaguchi, S. Ikeuchi, S. Ogasawara, N. Yamada, R. Ikeda, I. Ogawa, T. Idehara, Phys. Rev. Lett. (2012) https://doi.org/10.1103/PhysRevLett.109.155001
5) K. Felch, M. Blank, P. Borchard, S. Cauffman, M. Rosay, L. Tometich, Proc. IEEE Int. Vac. Electron. Conf. (2013) https://doi.org/10.1109/IVEC.2013.6571048
6) K.D. Hong, G.F. Brand, T. Idehara, J. Appl. Phys. (1993) http://dx.doi.org/10.1063/1.354265
7) D. Sun, H. Chen, G. Ma, W. Lei, H. Chen, F. Meng, J Infrared Millim. Terahertz Waves (2014) https://doi.org/10.1007/s10762-014-0064-1
8) G.S. Nusinovich, R. Pu, V. L. Granatstein, Appl. Phys. Lett. (2015) https://doi.org/10.1063/1.4926410
9) Q. Zhao, S. Yu, T. Zhang, IEEE Trans. Electron Devices (2017) https://doi.org/10.1109/TED.2017.2756635
10) M.M. Melnikova, A.G. Rozhnev, N.M. Ryskin, Y. Tatematsu, M. Fukunari, Y. Yamaguchi, T. Saito, IEEE Trans. Electron Devices (2017) https://doi.org/10.1109/TED.2017.2764874
11) I.V. Bandurkin, M.Yu. Glyavin, S.V. Kuzikov, P.B. Makhalov, I.V. Osharin, A.V. Savilov, IEEE Trans. Electron Devices (2017) https://doi.org/10.1109/TED.2017.2731982
12) Yu.S. Oparina, A.V. Savilov, J. Infrared Millim. Terahertz Waves (2018) https://doi.org/10.1007/s10762-018-0499-x
13) V.I. Shcherbinin, G.I. Zaginaylov, V.I. Tkachenko, "Cavity with distributed dielectric coating for subterahertz second-harmonic gyrotron," Problems Atomic Sci. Technol. 6 (106), 255 (2016).
14) V.I. Shcherbinin, V.I. Tkachenko, J. Infrared Millim. Terahertz Waves, (2017) https://doi.org/10.1007/s10762-017-0386-x
15) T.I. Tkachova, V.I. Shcherbinin, V.I. Tkachenko, J. Infrared Millim. Terahertz Waves (2019) https://doi.org/10.1007/s10762-019-00623-y
16) K.A. Avramides, C.T. Iatrou, J.L. Vomvoridis, "Design considerations for powerful continuous-wave second-cyclotron-harmonic coaxial-cavity gyrotrons," IEEE Trans. Plasma Sci. (2004) https://doi.org/10.1109/TPS.2004.828781
17) K.A. Avramides, J.L. Vomvoridis, C.T. Iatrou, AIP Conference Proceedings (2006) https://doi.org/10.1063/1.2158787
18) V.I. Shcherbinin, V.I. Tkachenko, K.A. Avramidis, J. Jelonnek, IEEE Trans. Electron Devices (2019) https://doi.org/10.1109/TED.2019.2944647
19) V.I. Shcherbinin, Y.K. Moskvitina, K.A. Avramidis and J. Jelonnek, IEEE Trans. Electron Devices (2020) https://doi.org/10.1109/TED.2020.2996179
20) S. Ruess, K. A. Avramidis, M. Fuchs, G. Gantenbein, Z. Ioannidis, S. Illy, J. Jin, P.C. Kalaria, T. Kobarg, I.Gr. Pagonakis, T. Ruess, T. Rzesnicki, M. Schmid, M. Thumm, J. Weggen, A. Zeinand, J. Jelonnek, Int. J. Microwave Wireless Technol. (2018) https://doi.org/10.1017/S1759078718000144
21) S. Illy, K.A. Avramidis, G. Gantenbein, Z. Ioannidis, J. Jin, P. C. Kalaria, I.Gr. Pagonakis, S. Ruess, T. Ruess, T. Rzesnicki, M. Thumm, J. Jelonnek, EPJ Web Conf. (2019) https://doi.org/10.1051/epjconf/201920304005
22) C.T. Iatrou, S. Kern, A.B. Pavelyev, IEEE Trans. Microw. Theory Techn. (1996) https://doi.org/10.1109/22.481385
23) C.T. Iatrou, IEEE Trans. Plasma Sci. (1996) https://doi.org/10.1109/27.532942
24) J.J. Barroso, R.A. Correa, P.J. Castro, IEEE Trans. Microw. Theory Techn (1998) https://doi.org/10.1109/22.709460.
25) La Agusu, T. Idehara, H. Mori, T. Saito, I. Ogawa, S. Mitsudo, Int. J Infrared Millim. Waves (2007) http://dx.doi.org/10.1007/s10762-007-9215-y.
26) C. Torrezan, S.T. Han, I. Mastovsky, M. A. Shapiro, J.R. Sirigiri, R.J. Temkin, A.B. Barnes, R.G. Griffin, IEEE Trans. Plasma Sci. (2010) http://dx.doi.org/10.1109/TPS.2010.2046617
27) S.K. Jawla, R.G. Griffin, I.A. Mastovsky, M.A. Shapiro and R.J. Temkin, IEEE Trans. Electron Devices (2020) https://doi.org/10.1109/TED.2019.2953658
28) V.I. Shcherbinin, T.I. Tkachova, V.I. Tkachenko, IEEE Trans. Electron Devices (2018) https://doi.org/10.1109/TED.2017.2769219
29) P.J. Castro, J.J. Barroso, R.A. Correa, Int. J Infrared Millim. Waves (1993) https://doi.org/10.1007/BF02096381
30) Y.J. Huang, K.R. Chu, M. Thumm, Phys. Plasmas (2015) http://dx.doi.org/10.1063/1.4905627
31) T. Saito, N. Yamada, S. Ikeuti, S. Ogasawara, Y. Tatematsu, R. Ikeda, I. Ogawa, T. Idehara, V.N. Manuilov, T. Shimozuma, S. Kubo, M. Nishiura, K. Tanaka, K. Kawahata, Phys. Plasmas (2012) https://doi.org/10.1063/1.4729316

32) V.I. Shcherbinin, G.I. Zaginaylov, V I. Tkachenko, Problems Atomic Sci. Technol. 4 (98), 89 (2015)
33) V.I. Shcherbinin, B.A. Kochetov, A.V. Hlushchenko, V.I. Tkachenko, IEEE Trans. Microw. Theory Techn. (2019) https://doi.org/10.1109/TMTT.2018.2882493
34) J. Genoud, S. Alberti, J.-Ph. Hogge, I.G. Tigelis, G.P. Latsas, I.G. Chelis, Phys. Plasmas (2019) https://doi.org/10.1063/1.5130637
35) V.I. Shcherbinin, A.V. Hlushchenko, A.V. Maksimenko, V.I. Tkachenko, IEEE Trans. Electron Devices, (2017) https://doi.org/10.1109/TED.2017.2730252
36) D.B. McDermott, D.S. Furuno, N.C. Luhmann, Int. J Infrared Millim. Waves (1983) https://doi.org/10.1007/BF01009701
37) V.I. Shcherbinin, G.I. Zaginaylov, V.I. Tkachenko, Prog. Electromagn. Res. M, (2017) https://doi.org/10.2528/PIERM16110902
38) K.A. Avramides, Design and simulation of coaxial gyrotrons (laying emphasis on second-harmonic operation) (Ph. D. Thesis, National Technical University of Athens, Athens, 2006), https://www.didaktorika.gr/eadd/handle/10442/16296?locale=en (in Greek)
39) E. Savrun, V. Nguyen, D.K. Abe, Proc. IEEE Int. Vac. Electron. Conf. (2002) https://doi.org/10.1109/IVELEC.2002.999246
40) J.P. Calame, M. Garven, D. Lobas, R.E. Myers, F. Wood, D.K. Abe, Proc. IEEE Int. Vac. Electron. Conf. (2006) https://doi.org/10.1109/IVELEC.2006.1666172
41) J.P. Calame, M. Garven, B.G. Danly, B. Levush, K.T. Nguyen, IEEE Trans. Electron Devices (2002) https://doi.org/10.1109/TED.2002.801254
42) Y. Xu, M. Sun, T. Peng, J. Wang, Y. Luo, R. Yan, W. Jiang, G. Liu, H. Li, IEEE Trans. Electron Devices (2019) https://doi.org/10.1109/TED.2019.2894537
43) E. Borie, O. Dumbrajs, Int. J. Electron. (1986) https://doi.org/10.1080/00207218608920768
44) D. Wagner, G. Gantenbein, W. Kasparek, M. Thumm, Int. J. Infrared Millim. Waves (1995) https://doi.org/10.1007/BF02274811
45) G.I. Zaginaylov, V.I. Shcherbinin, K. Schünemann, M. Yu Glyavin, Proc. 8th MSMW (2013) https://doi.org/10.1109/MSMW.2013.6622127
46) A.V. Maksimenko, G.I. Zaginaylov, V.I. Shcherbinin, Physics of Particles and Nuclei Letters (2015) https://doi.org/10.1134/S1547477115020168
47) A.V. Maksimenko, V.I. Shcherbinin, V.I. Tkachenko, J. Infrared Millim. Terahertz Waves (2019) https://doi.org/10.1007/s10762-019-00589-x
48) A.V. Maksimenko, V.I. Shcherbinin, A.V. Hlushchenko, V.I. Tkachenko, K.A. Avramidis and J. Jelonnek, IEEE Trans. Electron Devices (2019) https://doi.org/10.1109/TED.2019.2893888
49) G.S. Nusinovich, Introduction to the physics of gyrotrons (The Johns Hopkins University Press, Baltimore, 2004), p. 62.
50) G. Gantenbein, G. Dammertz, J. Flamm, S. Illy, S. Kern, G. Latsas, B. Piosczyk, T. Rzesnicki, A. Samartsev, A. Schlaich, M. Thumm, I. Tigelis, IEEE Trans. Plasma Sci (2010) https://doi.org/10.1109/TPS.2010.2041366
51) G. Chelis, K.A. Avramidis, Z.C. Ioannidis, I.G. Tigelis, IEEE Trans. Electron Devices, (2018) https://doi.org/10.1109/TED.2017.2784198
52) M. Thumm, Int. J. Infrared Millim. Waves, (1998) https://doi.org/10.1023/A:1022514528711
53) V.V. Parshin, V.N. Derkach, B.M. Garin, R. Heidinger, J. Molla, V.G. Ralchenko, S.I. Tarapov, I. Danilov, S.E. Myasnikova, V.I. Polyakov, A.I. Rukovishnikov, Proc. IRMMW-THz (2005) https://doi.org/10.1109/ICIMW.2005.1572387
54) V.V. Parshin, M.Y. Tretyakov, M.A. Koshelev, E.A. Serov, IEEE Sensors J., (2013) https://doi.org/10.1109/JSEN.2012.2215315

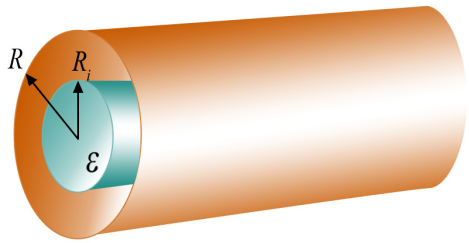

Fig. 1 Metal cylindrical waveguide loaded with a coaxial dielectric rod.

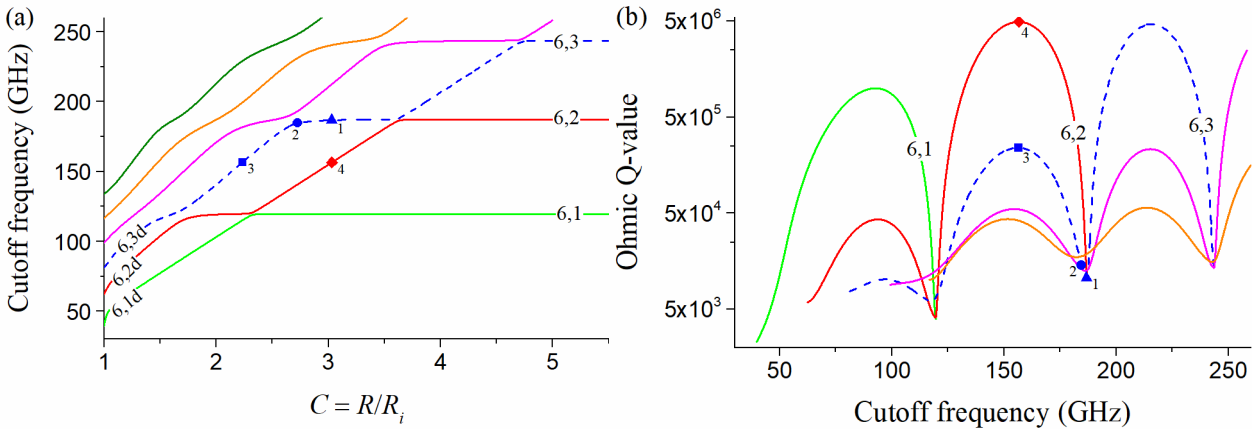

Fig. 2 (a) Cutoff frequencies and (b) ohmic Q-values of the $TE_{6,n}$ modes of a cylindrical metal waveguide loaded with a coaxial dielectric rod ($R = 2.99$ mm, $\varepsilon_r = 9$, $\tan\delta = 0$, $\sigma = 2.9\times10^7$ S/m).

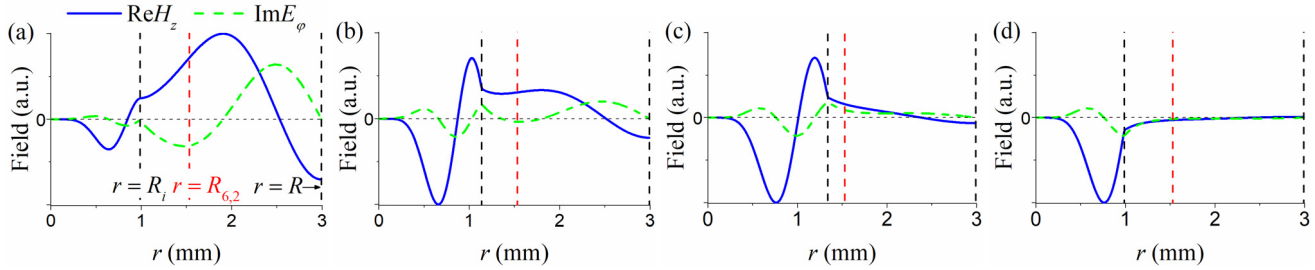

Fig. 3 Radial field structure inside a dielectric-loaded circular waveguide for TE modes with complex eigenvalues, which are shown by symbols a) 1, b) 2, c) 3, and d) 4 in Fig. 1. Here $R_{6,2}$ denotes the caustic radius of the $TE_{6,2}$ mode.

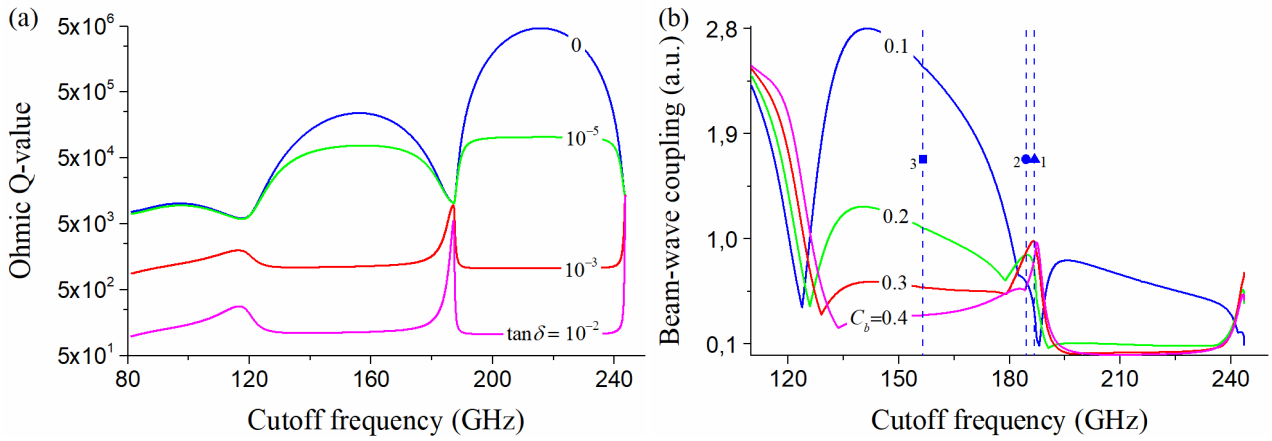

Fig. 4 (a) Ohmic Q-value and (b) normalized beam-wave coupling coefficients versus cutoff frequency of the $TE_{6,3}$ mode (see dashed blue line in Fig. 1) for different $\tan\delta$ and C_b, respectively

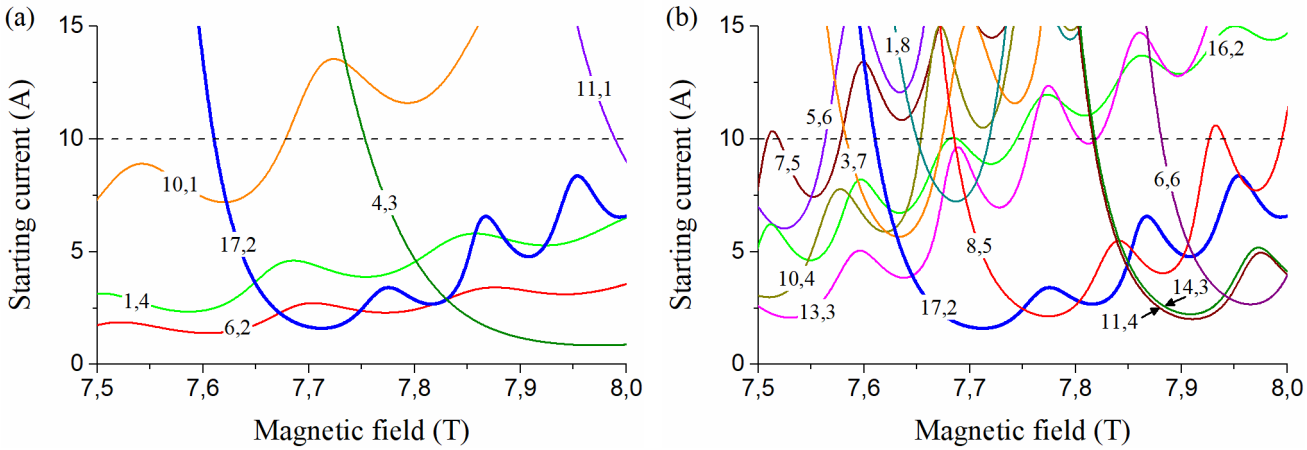

Fig. 5 Starting currents of the operating $TE_{17,2}$ mode and (a) first– and (b) second–harmonic competing modes of the 0.39-GHz second-harmonic gyrotron [4, 31].

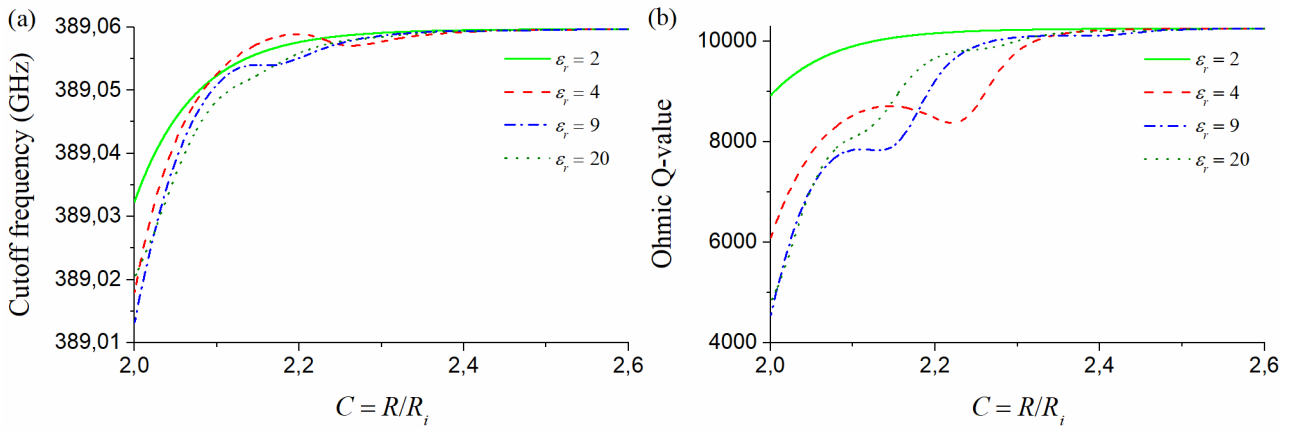

Fig. 6 (a) Cutoff frequency and (b) ohmic Q-value of the $TE_{17,2}$ mode versus the radius ratio C of a metal cylindrical waveguide loaded with a coaxial dielectric rod for different ε_r ($R = 2.99$ mm, $\tan\delta = 0.05$, $\sigma = 2.9\times10^7$ S/m).

Table I

Cutoff frequencies (f_c) and ohmic Q-values (Q_{ohm}) of TE modes of a dielectric-loaded waveguide for different R_i ($R = 2.99$ mm, $\varepsilon_r = 9$, $\tan\delta = 0.05$)

		$R_i = 0$		$R_i = 1.30$ mm		$R_i = 1.18$ mm	
Mode	$R_{m,n}$, mm	f_c,GHz	Q_{ohm}	f_c,GHz	Q_{ohm}	f_c,GHz	Q_{ohm}
17,2	2.085	389.06	10254	389.06	10079	389.06	10245
14,3	1.674	398.97	13872	398.49	766	398.88	3601
13,3	1.632	380.09	13849	379.30	466	379.90	1968
4,3	0.943	202.37	12961	200.63	41	205.59	41
6,2	1.529	187.25	10226	183.47	103	187.18	89
6,2d	1.529	–	–	160.92	23	176.80	27

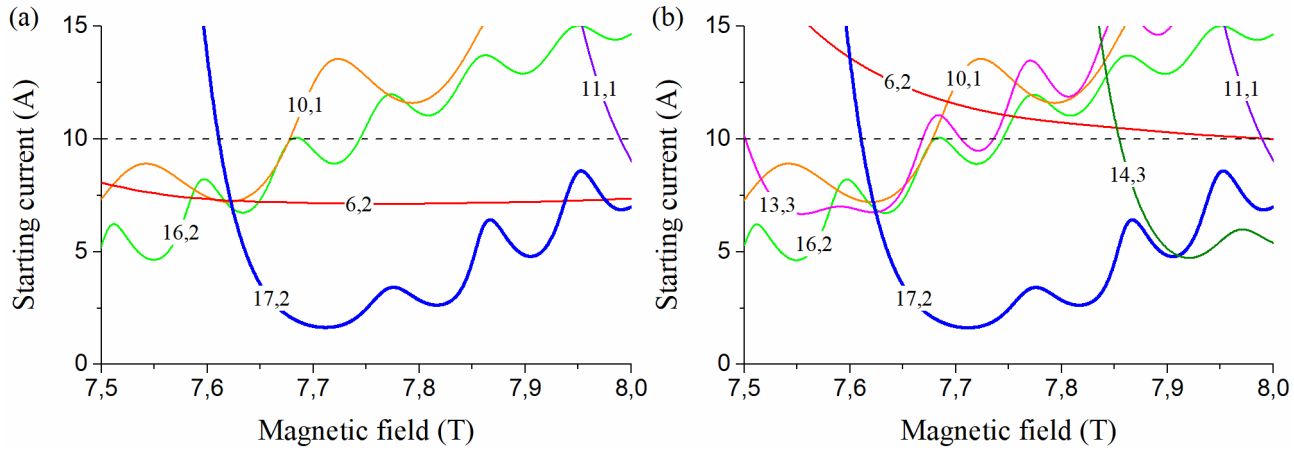

Fig. 7 Starting currents of the operating and competing modes of the 0.39-GHz second-harmonic gyrotron equipped with the dielectric-loaded cavity for (a) $R_i = 1.3$ mm and (b) $R_i = 1.18$ mm ($\varepsilon_r = 9$, $\tan\delta = 0.05$).

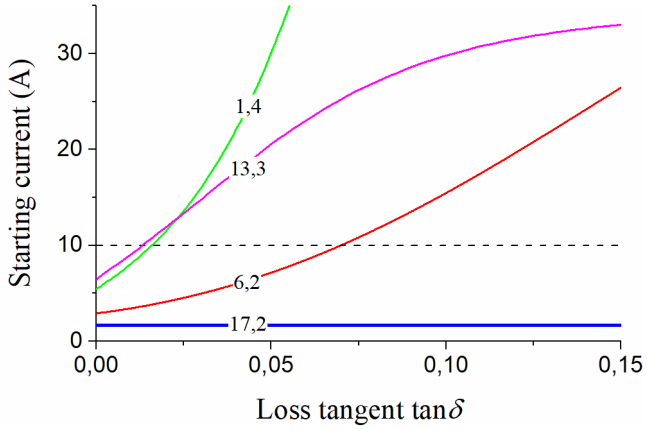

Fig. 8 Effect of dielectric losses on the starting currents of the 0.39-THz second-harmonic gyrotron for $B_0 = 7.7$ T, $\varepsilon_r = 9$, and $R_i = 1.3$ mm.